ELSEVIER

Chemical Physics 210 (1996) 353–366

Chemical Physics

Linear and nonlinear optical response of dimethyl-amino-nitro-stilbene (DANS): coupled oscillator representation versus sum-over-states picture

D. Beljonne [a], J.L. Brédas [a,*], G. Chen [b], S. Mukamel [b]

[a] *Service de Chimie des Matériaux Nouveaux, Centre de Recherche en Electronique et Photonique Moléculaires, Université de Mons-Hainaut, Place du Parc 20, 7000 Mons, Belgium*

[b] *Department of Chemistry, University of Rochester, Rochester, NY 14627, USA*

Received 22 January 1996

Abstract

The first-, second-, and third-order optical polarizabilities of dimethyl-amino-nitro-stilbene (DANS) have been calculated on the basis of a coupled oscillator picture and compared to the results obtained within the sum-over-states formalism. The two approaches leąd to a very similar description for both static and dynamic responses. The correspondence between the nature of the dominant oscillators and the essential excited states contributing primarily to the linear and nonlinear optical response is emphasized.

1. Introduction

As a consequence of their highly delocalized π-electron clouds, conjugated organic polymers and oligomers possess very large optical nonlinearities, which make them suitable for a wide range of applications in the general field of information technology [1–4]. The engineering of new optical materials with improved characteristics requires shedding light on the fundamental relationships between the molecular structure and the microscopic properties. In this context, quantum-chemical calculations prove to be useful by helping in understanding the microscopic origin of the optical nonlinearities.

Quantum chemists traditionally calculate the molecular polarizabilities by using sum-over-states (SOS) expressions derived from perturbation theory [5]. The nonlinearities are then expanded using the many-body electronic eigenstates, and expressed in terms of the eigenvalues (state energies) and matrix elements of the dipole operator (transition and state dipole moments). The finite-field (FF) technique, which is based on derivations to various orders of the Stark energy (total energy in the presence of a perturbing electric field) has also been widely used to calculate the static nonlinearities [6–9]. The main advantages of the SOS formalism over the FF method are that the former approach allows: (i) to identify the nature of the relevant excited states dominating the optical response [10–13]; (ii) to easily incorporate the frequency dependence of the polarizabilities for a variety of processes [14–17]; and (iii) to get a physical insight into the origin of the response by investigating the importance of different contribu-

* Corresponding author.

PII S0301-0104(96)00170-X

tions such as electron correlation, through the description of the excited states [18]. The major drawback of both SOS and FF techniques is the need to compute the global eigenstates, which, despite the tremendous progress in computational methods, remains a demanding objective.

Recently, another strategy based on a coupled oscillators picture has gained popularity to calculate the molecular polarizabilities [19–21]. Here, the optical response is evaluated from the single-electron reduced density matrix obtained by solving the equations of motion in the time-dependent Hartree–Fock (TDHF) approximation. The equations of motion of the density matrix can be mapped onto a set of coupled harmonic oscillators, which provides a seemingly very different physical picture of the mechanisms involved in the description of the nonlinearities. Within this formalism, the optical properties are directly related to the motions of electron–hole pairs, without ever introducing the many-body wavefunctions. Thus, the necessary computational effort is greatly reduced compared to the one required in the SOS and FF approaches.

Moreover, we should keep in mind that the third-order response as obtained from SOS calculations usually results from dramatic cancellations between very large positive and negative contributions [10–13]; therefore, unbalanced description of these contributions, as a consequence of truncation in the summation over the excited states or a lack of electron correlation in the description of the eigenstates, can cause very large fluctuations in the resulting value of the polarizability. Such a problem is avoided in the oscillator representation, where the interferences between the various contributions to the nonlinearities are naturally built in from the beginning [19–21]. The coupled electronic oscillator (CEO) picture has been successfully applied to predict the saturation length of the third-order polarizability in polyenes [19,20] and to uncover the structure/property relationships in push–pull polyenes [21].

Although the TDHF approach describes quantum fluctuations around the Hartree–Fock ground state and therefore takes into account some correlation effects [22,23], it is not clear yet to what extent these effects are included in the CEO formalism. Another important question is whether the relevant oscillators in the expression of the nonlinearities can be connected to the essential excited states unraveled by the SOS calculations. To get insight into these two issues, we have applied the two techniques (SOS and CEO) to evaluate the first-, second-, and third-order polarizabilities of a prototype molecule, dimethylamino-nitro-stilbene (DANS). The reasons why we have focused on DANS for such a comparison are the following: (i) the finite size of the molecule allows an accurate description of the excited states by conventional configuration interaction (CI) techniques, and therefore a precise estimation of its linear and nonlinear response by the SOS formalism [16]; (ii) as a consequence of symmetry breaking induced by the end groups, DANS shows both second-, and third-order nonlinearities; a richer information can thus be expected from the analysis of its optical response with respect to that provided by the study of centrosymmetric compounds (the comparison between the results afforded by the two theoretical schemes for centrosymmetric molecules is discussed elsewhere in the case of octatetraene [24]); and (iii) with large quadratic and cubic polarizabilities, DANS is a molecule of choice for potential applications [25].

2. Methodology

On the basis of the ground-state geometry of the DANS molecule, optimized at the Hartree–Fock semiempirical Austin Model 1 (AM1) [26] level, we describe the lowest singlet excited states by means of the intermediate neglect of differential overlap (INDO) Hamiltonian [27] coupled to the multireference double configuration interaction (MRD-CI) technique [28]. As pointed out by Tavan and Schulten in the case of polyenes, for systems of the size of DANS, the MRD-CI scheme provides transition energies for the lowest excited states to a degree of precision close to that obtained within the quadruple CI approach [29].

The excitation energies, state and transition dipole moments evaluated by the INDO/MRD-CI approach are then included in the sum-over-states formalism [5,30] to estimate the chain-axis component of the first-, second-, and third-order polarizabilities, respectively α_{xx}, β_{xxx}, and γ_{xxxx}. The linear and nonlinear dispersion curves are simulated by calcu-

lating the optical response for different frequencies, assuming the same damping factor (0.1 eV) for all excited states.

As for the coupled electronic oscillator (CEO) picture, we start with the Pariser–Parr–Pople (PPP) Hamiltonian, which is known to capture the essential electronic properties of the π-electronic systems [19–21]. We model the donor and acceptor moieties of DANS by adding one orbital at each end of the conjugated chain, as previously described [21]. For the sake of consistency, we use the same parameters to describe the electron–phonon and electron–electron interactions within the PPP model as those adopted to calculate the optical nonlinearities of polyenes [24]. To allow for a direct comparison to the SOS results, the AM1 geometry of DANS is used as input for the PPP calculations.

We then follow the dynamics of the single electron reduced density matrix, $\rho_{nm}(t) = \langle c_m^+ c_n \rangle$ (where c_m^+ [c_n] is the creation [annihilation] operator for a π electron at site m), in the time-dependent Hartree–Fock (TDHF) approximation. It is shown in Ref. [21] that the equations of motion of the density matrix map the electronic system onto a collection of anharmonic oscillators with frequencies Ω_v. The chain-axis component of nth order polarizability χ_n (where $\chi_1 = \alpha_{xx}$; $\chi_2 = \beta_{xxx}$, and $\chi_3 = \gamma_{xxxx}$) can then be expressed in terms of these oscillators:

$$X_n = \sum_v d_v Q_v^{(n)} / F^n, \tag{1}$$

where F is the external field, $Q_v^{(n)}$ represents the amplitude of the vth oscillator to nth order in the field, and d_v is the dipole moment,

$$d_v = -\sum_m 2\sqrt{2}\, ex(m) U_{mm,v}^{-1}, \tag{2}$$

where $x(m)$ is the coordinate of the mth atom in the chain direction and $U_{mn,v}^{-1}$ is the mn component of the eigenvector associated to oscillator v. The oscillator amplitudes $Q_v^{(n)}$ are calculated successively, order by order in the field F, and can be expressed in terms of couplings between the oscillators and the field or among oscillators, as a result of the Coulomb interactions. For the dynamic response, we adopt the same value (0.1 eV) for the damping factor as the one considered in the SOS calculations.

3. Linear and nonlinear optical response of DANS

DANS is a typical charge-transfer molecule, formed by a conjugated bridge (a stilbene unit) substituted at one end by an electron-donating moiety (the dimethylamino group) and by an electron-withdrawing moiety (the nitro group) at the other end. As such, the molecule possesses both large second- and third-order nonlinearities [16,25]. The amplitude of the optical response is determined by the amount of charge transfer, which is controlled in our PPP model by the atomic energies of the end sites, ε_D (for the donor orbital) and ε_A (for the acceptor orbital) [21]. Fig. 1 shows the ground-state π charge distribution obtained by the PPP/CEO scheme for various couples of ε_D and ε_A values (in each case, ε_A is tuned to give rise to an absolute π charge on the acceptor site that is half the value evaluated for the donor site, as obtained from the INDO/MRD-CI calculations). The evolution with ε_D of the first-, second-, and third-order polarizabilities, as calculated at the PPP/CEO level, is illustrated in Fig. 2. From Figs. 1 and 2, we see that, for

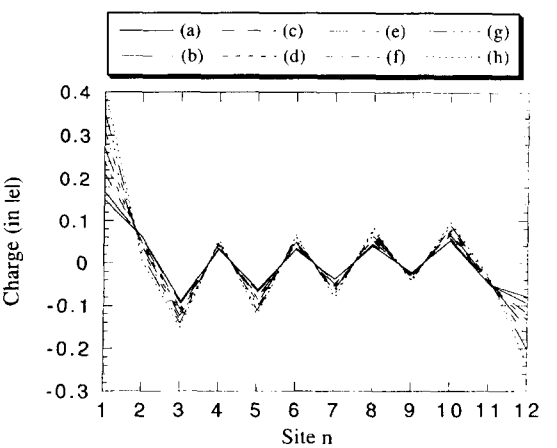

Fig. 1. Charge distribution calculated by the PPP/CEO scheme for: (a) $\varepsilon_D = -2.0$ eV and $\varepsilon_A = 3.2$ eV; (b) $\varepsilon_D = -1.5$ eV and $\varepsilon_A = 2.4$ eV; (c) $\varepsilon_D = -0.5$ eV and $\varepsilon_A = 1.5$ eV; (d) $\varepsilon_D = 0.0$ eV and $\varepsilon_A = 1.0$ eV; (e) $\varepsilon_D = 0.5$ eV and $\varepsilon_A = 0.5$ eV; (f) $\varepsilon_D = 1.0$ eV and $\varepsilon_A = 0.0$ eV; (g) $\varepsilon_D = 1.5$ eV and $\varepsilon_A = -0.5$ eV; and (h) $\varepsilon_D = 2.0$ eV and $\varepsilon_A = -1.0$ eV. Site 1 corresponds to the donor orbital, site 12 to the acceptor orbital. For the stilbene unit, we present the average value of the charges on the sites, that would be equivalent under D_{2h} symmetry.

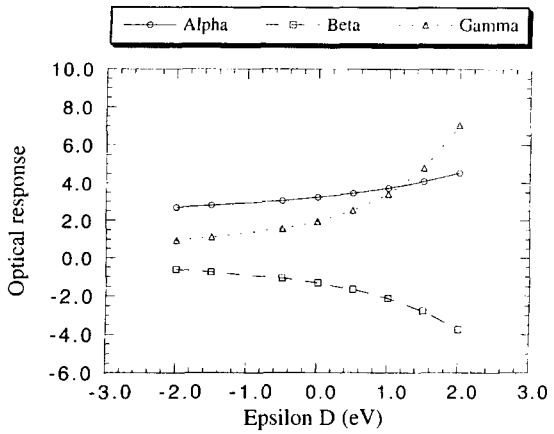

Fig. 2. Dependence upon ε_D of the first- (α_{xx}, in e Å^2 V^{-1}), second- (β_{xxx}, in e Å^3 V^{-2}), and third-order (γ_{xxxx}, in e Å^4 V^{-3}) polarizabilities of DANS, as calculated at the PPP/CEO level. Note that, in each case, the ε_A value is adjusted to lead to an absolute charge on the acceptor site that is half the value calculated for the donor.

the range of ε_D values considered here, the larger the charge transfer from the donor to the acceptor through the conjugated bridge, the larger the optical response; this dependence is particularly pronounced for the quadratic and cubic responses and has been investigated in detail previously [21,31].

We find the best agreement to the INDO/MRD-CI charge distribution by considering $\varepsilon_D = -2.0$ eV and $\varepsilon_A = 3.2$ eV in the PPP model; we will thus focus on the results obtained for these parameters in the rest of the discussion. In Table 1, we list the static values of α_{xx}, β_{xxx}, and γ_{xxxx}, as evaluated by the INDO/MRD-CI/SOS and PPP/CEO approaches. In view of the completely different methodology adopted in the two techniques, the agreement between the two sets of results is very good. Note that an even better agreement with the SOS results could be obtained by adjusting the PPP

Table 1
Static values of the chain-axis component of the first- (α_{xx}, in e Å^2 V^{-1}), second- (β_{xxx}, in e Å^3 V^{-2}), and third-order (γ_{xxxx}, in e Å^4 V^{-3}) polarizabilities of DANS, as calculated by the INDO/MRD-CI/SOS and PPP/CEO schemes

	α_{xx}	β_{xxx}	γ_{xxxx}
INDO/MRD-CI/SOS	2.17	−1.17	1.10
PPP/CEO	2.70	−0.65	0.93

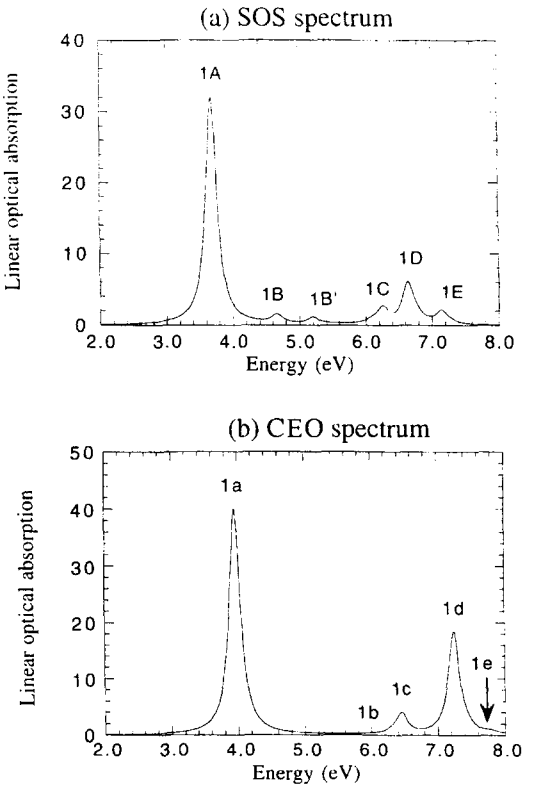

Fig. 3. Linear optical absorption spectrum of DANS (Im(α_{xx}), in e Å^2 V^{-1}), simulated by: (a) the INDO/MRD-CI/SOS formalism; and (b) the PPP/CEO scheme.

parameters to the DANS molecule (we recall that we use the same parameters as those considered for polyenes [24]) but this goes beyond the scope of the present calculations.

The linear absorption spectrum (imaginary part of α_{xx}) of DANS, simulated by the SOS and CEO schemes, is given in Fig. 3. The SOS spectrum shows six resonant peaks (denoted 1A, 1B, 1B′, 1C, 1D, and 1E on Fig. 3a) forming three absorption bands: (i) a very intense low-energy band dominated by peak 1A and centered around 3.7 eV; (ii) a high-energy band composed of three features (1C, 1D, and 1E) located at 6.2, 6.6, and 7.2 eV; and (iii) a weak intermediate band with two peaks (1B and 1B′) at 4.7 and 5.2 eV. A rather similar optical absorption spectrum is obtained within the PPP/CEO formalism (Fig. 3b): the spectrum is dominated by an intense peak (1a, at 4.0 eV) and shows also a high-energy band with three features (1c, 1d, and 1e,

at 6.4, 7.2, and 7.8 eV, respectively); however, in opposite to the SOS results, the intermediate optical absorption band (1b, at 5.9 eV) is too weak to be isolated from the non-resonant background. We note also that all the features calculated at the PPP/CEO level are systematically blue-shifted (by 0.3–0.6 eV) with respect to the INDO/MRD-CI/SOS calculations; again, this discrepancy can be accounted for by the different parameters considered in the two Hamiltonians (PPP and INDO).

The SOS and CEO second-harmonic generation (SHG) frequency-dependent curves (Fig. 4) can also be decomposed into three parts: (i) a dominant high-energy band; (ii) a less intense low-energy peak; and (iii) weak features in between. On the basis of the energy and relative intensity of the different resonances, we tentatively associate peaks 2a (at 2.0 eV); 2b (at 3.0 eV); 2c (at 3.2 eV); and 2d (at 3.9 eV) on the CEO simulated SHG spectrum (Fig. 4b) to,

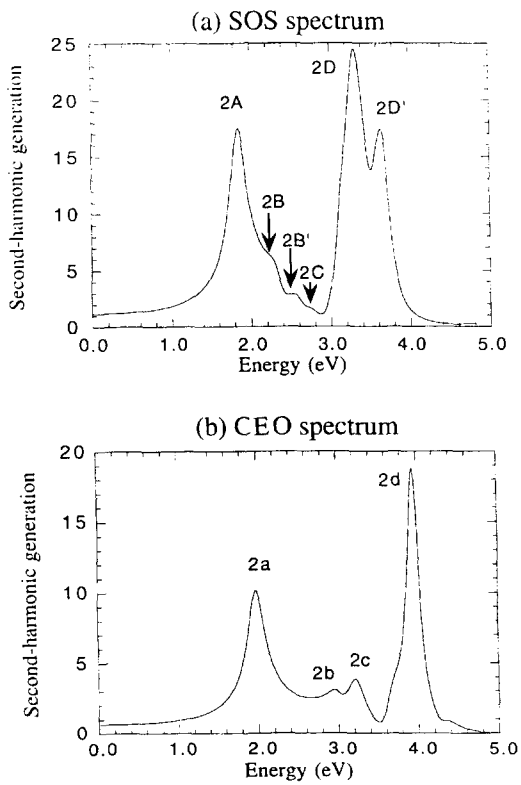

Fig. 4. Second-harmonic generation frequency-dependent curve of DANS (β_{xxx}, in e Å^3 V^{-2}), simulated by: (a) the INDO/MRD-CI/SOS formalism; and (b) the PPP/CEO scheme.

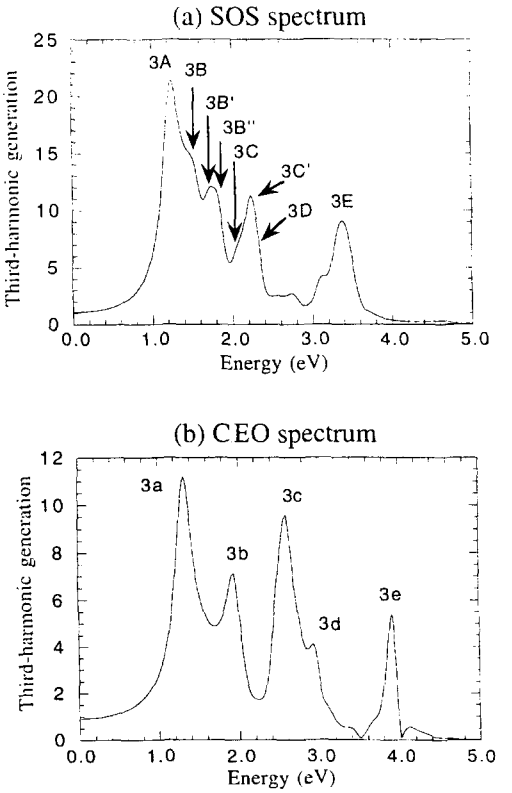

Fig. 5. Third-harmonic generation frequency-dependent curve of DANS (γ_{xxxx}, in e Å^4 V^{-3}), simulated by: (a) the INDO/MRD-CI/SOS formalism; and (b) the PPP/CEO scheme.

respectively, the 2A (at 1.8 eV); 2B (at 2.3 eV) and 2B′ (at 2.6 eV); 2C (at 2.8 eV); and 2D (at 3.3 eV) and 2D′ (at 3.7 eV) features on the corresponding SOS dispersion curve (Fig. 4a).

As in the case of second-harmonic generation, we find a good agreement between the general shape of the third-harmonic generation (THG) frequency-dependent curves, evaluated by applying the SOS and CEO techniques (Fig. 5). With respect to the SHG dispersion curve, the THG spectrum presents a richer structure, which is expected since for an asymmetric molecule like DANS, both one-, two-, and three-photon resonances can occur for the same excited state. From the position and height of the resonances, we can reasonably assume that peaks 3a (at 1.3 eV); 3b (at 2.0 eV); 3c (at 2.6 eV); 3d (at 2.9 eV); and 3e (at 3.9 eV) calculated by the CEO scheme (Fig. 5b) correspond to the features labeled as 3A (at 1.2 eV);

3B (at 1.5 eV), 3B′ (at 1.7 eV), and 3B″ (at 1.8 eV); 3C (at 2.1 eV) and 3C′ (at 2.2 eV); 3D (at 2.3 eV); and 3E (at 3.4 eV) on the THG dispersion curve simulated at the SOS level (Fig. 5a). It is worth stressing that, for both SHG and THG processes, establishing a correspondence between the resonances calculated by the two techniques requires in some cases to associate to a given peak on the CEO spectrum several features on the SOS dispersion curve. In order to clarify this point and also to allow for an assignment of the different resonant peaks, the analysis of the linear and nonlinear optical response in terms of the relevant excited states/oscillators is required.

4. Dominant excited states/oscillators analysis

We first focus on the off-resonant polarizabilities. In the SOS picture, the linear and nonlinear response is built by summing the contributions associated to different channels. For a noncentrosymmetric structure, these channels involve the electronic couplings between the excited states through the transition dipole moments as well as the charge transfer occurring upon excitation and related to the difference between the state dipole moments. The relevant channels in the description of the static first-, second-, and third-order polarizabilities of DANS are sketched in Fig. 6 and their contributions are collected in Table 2. To gain insight into the nature of the excited states dominating the optical response, we collect in Table 3 the largest CI expansion coefficients associated to these states; these coefficients correspond to the weight of the different electronic excitations or configurations of each eigenstate. As in phenylene vinylene oligomers [32], the molecular orbitals of DANS can be classified in two categories: (i) orbitals delocalized over the whole conjugated system (hereafter denoted by the index d); and (ii) orbitals confined on the benzene rings (hereafter denoted by the index l; three types of configurations

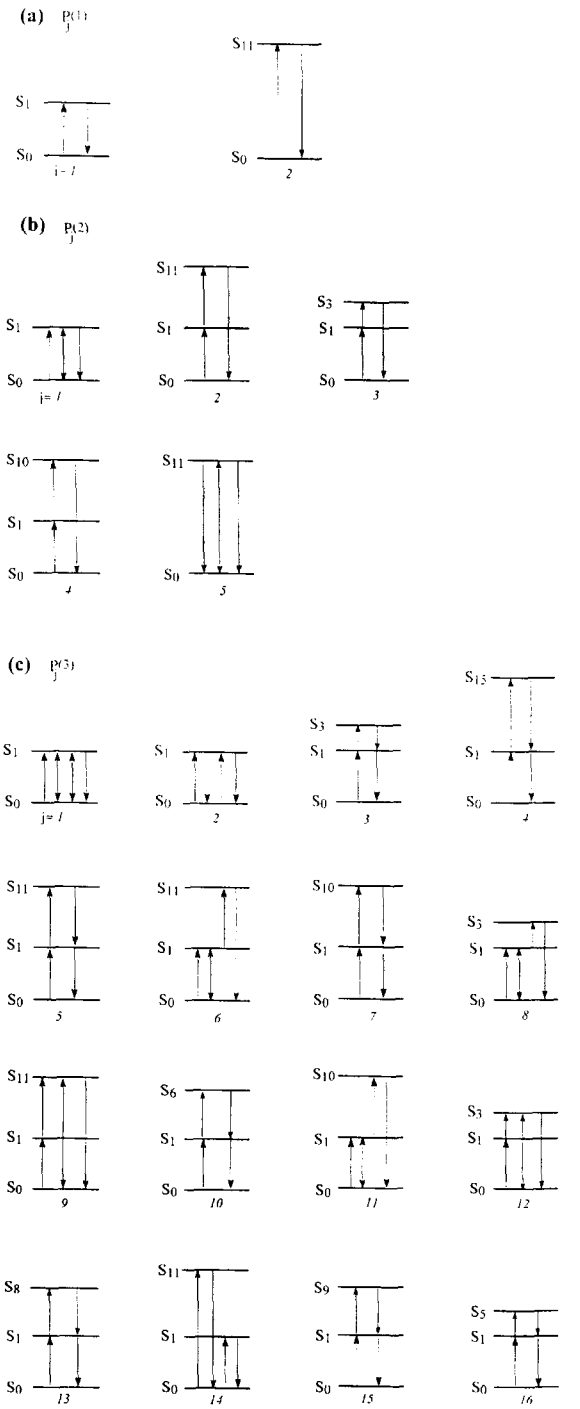

Fig. 6. Sketch of the dominant channels, $P_j^{(n)}$, in the description of the static nth-order polarizability of DANS, as obtained from the INDO/MRD-CI/SOS calculations. S_i denotes eigenstate i, where i is the state quantum number (S_0 is the ground state). Up or down arrows represent transition dipole moments coupling the eigenstates and double arrows refer to the dipole moment differences with the ground state. The contributions associated to these channels are given in Table 2.

can be built from these orbitals: (i) excitations from an occupied delocalized level to an occupied delocalized level (noted $F_d \rightarrow E_d$); (ii) mixed-type excitations involving both extended and confined molecular orbitals ($F_d \rightarrow E_l$ and $F_l \rightarrow E_d$); and (iii) transitions between localized levels ($F_l \rightarrow E_l$).

From Fig. 6 and Tables 2 and 3, we can summarize the SOS results as follows.

(i) The linear response of DANS is dominated by the lowest excited state, S_1, mainly described by a single excitation from the highest occupied molecular orbital (HOMO) to the lowest unoccupied molecular orbital (LUMO). Other contributions are at least one order of magnitude smaller and involve higher-lying excited states with complex wavefunctions.

Table 2
Contributions of the main pathways, $P_j^{(n)}$, to the static value of the nth-order polarizability of DANS, as calculated by the INDO/MRD-CI/SOS scheme

$n=1$		$n=3$	
$P_j^{(1)}$	contribution (in e Å^2 V^{-1})	$P_j^{(3)}$	contribution (in e Å^4 V^{-3})
$j=1$	1.74	$j=1$	1.45
$j=2$	0.17	$j=2$	−0.82
$P_\Sigma^{(1)}$	1.91	$j=3$	0.40
$P_{tot}^{(1)}$	2.17	$j=4$	0.36
$n=2$		$j=5$	0.29
$P_j^{(2)}$	contribution (in e Å^3 V^{-2})	$j=6$	−0.20
$j=1$	−1.68	$j=7$	0.19
$j=2$	0.23	$j=8$	−0.13
$j=3$	0.15	$j=9$	−0.12
$j=4$	−0.11	$j=10$	0.11
$j=5$	−0.10	$j=11$	0.10
$P_\Sigma^{(2)}$	−1.24	$j=12$	−0.09
$P_{tot}^{(2)}$	−1.17	$j=13$	0.08
		$j=14$	−0.08
		$j=15$	0.07
		$j=16$	0.07
		$P_\Sigma^{(3)}$	1.21
		$P_{tot}^{(3)}$	1.10

All the channels giving rise to a contribution larger than 5% of the total response are included. We also indicate the sum of these contributions (including those of the channels obtained by changing the order of the different excitation processes), $P_\Sigma^{(n)}$, as well as the total response, $P_{tot}^{(n)}$.
The pathways are labeled according to Fig. 6.

(ii) S_1 is also the most relevant excited state in the description of the second-order molecular polarizability. The β_{xxx} value is mainly controlled by a pathway involving the difference in dipole moments between the ground state, S_0, and the excited state S_1; the large charge transfer associated to the $S_0 \rightarrow S_1$ excitation results from strong contributions of the donor [acceptor] orbitals to the HOMO [LUMO] level. Similar results have been found in push–pull polyenes [33] and form the basis of the two-state model as originally proposed by Chemla and Oudar [34]. As in the case of α_{xx}, other excited states contribute to a smaller extent to the β_{xxx} value. These can be classified in two groups: low-lying states (mainly S_3) formed by $F_d \rightarrow E_d$ types of excitation and high-lying states (mainly S_{10} and S_{11}) resulting from the mixing between the three types of transitions listed above.

(iii) The situation is more complex for the cubic nonlinearity, characterized by a larger number of significant channels. However, in a similar way as for the first- and second-order response, S_1 plays a major role in defining the third-order polarizability and is involved in all the relevant pathways. The other important excited states in the SOS expression of γ_{xxxx} form a low- (S_3 and S_5) and high-energy band (S_8, S_9, S_{10}, S_{11}, and S_{15}), with main contributions associated to S_3, S_{10}, S_{11}, and S_{15}. Note that, as these states present large transition dipole moments with S_1, they should correspond to the essential two-photon states ($2A_g$ and mA_g) included in the SOS model for the third-order response of symmetric conjugated systems [10–13]. We are currently investigating the optical nonlinearities of the stilbene molecule to check this hypothesis.

In the CEO representation, tree diagrams [35], which show how the oscillators couple successively, provide an alternative to the channel picture based on the electronic couplings between the excited states of the system. In first order, the relevant oscillators result from the coupling between the ground state and the perturbing electric field; in second order, the dominant first-order oscillators couple with the field and among themselves to produce the second-order oscillators; these couple to the first-order oscillators and with the field to give rise to the third-order oscillators. In Fig. 7, we use tree diagrams to illustrate how the nth-order oscillators, dominating the

nth-order polarizability of DANS, are built; the major contributions to the linear and nonlinear response resulting from these couplings are collected in Table 4. To allow for a direct comparison to the INDO/MRD-CI/SOS results, we have projected the relevant oscillators onto the Hartree–Fock molecular orbital basis set. Assuming an analogy between the excited states and oscillators, the projection coefficients, listed in Table 5, should correspond to the weights of the electronic configurations in the description of the excited states (Table 3).

From the comparison between the SOS (Tables 2 and 3, Fig. 6) and CEO (Tables 4 and 5, Fig. 7) results, the following conclusions can be drawn.

(i) Oscillator O_1 plays an overwhelming role in the description of the optical response of DANS, whatever the order in the field. O_1 is built mainly from the transition between the frontier molecular orbitals (HOMO and LUMO), and clearly corresponds to the S_1 excited state (note that the HOMO $-1 \rightarrow$ LUMO and HOMO $\rightarrow$ LUMO $+1$ excitations also participate to the description of both O_1 and S_1).

(ii) Coupling of O_1 with itself and with the electric field leads to higher-order oscillators with large contributions in the expression of the quadratic and cubic nonlinearities; among them, O'_1, O'_2, O'_3, and O'_4 are dominant. These oscillators result from intra-

Table 3
Main CI expansion coefficients associated to the excited states, S_i, dominating the optical response of DANS, as obtained from INDO/MRD-CI calculations

	S_1	S_3	S_5	S_6	S_8	S_9	S_{10}	S_{11}	S_{15}
μ_{0i}	8.6	1.7	1.5	0.41	−1.0	1.0	2.0	−3.6	0.33
$\mu_{ii} - \mu_{00}$	−11.4	−10.4	−7.3	−8.1	−8.4	−9.4	−9.7	−12.7	−10.4
E_{0i}	3.68	4.66	5.20	5.56	6.08	6.21	6.26	6.63	6.92
CI expansion coefficients									
$F_d \rightarrow E_d$									
$H_d \rightarrow L_d$	−0.84						0.21	−0.16	
$(H-1)_d \rightarrow L_d$	0.22		0.64	0.24			0.17	−0.37	
$H_d \rightarrow (L+1)_d$	−0.33	−0.74		−0.24	−0.18			0.18	
$(H-1)_d \rightarrow (L+1)_d$				0.22	0.22	0.28	−0.32	0.26	−0.48
$(H-5)_d \rightarrow L_d$	0.22				0.26	0.22	−0.16	−0.26	
$H_d \rightarrow (L+4)_d$		−0.31		0.56	0.31				0.27
$H_d \rightarrow (L+5)_d$				−0.36	0.48				
$H_d \rightarrow (L+8)_d$						−0.18			−0.20
$H_d \rightarrow (L+10)_d$						0.19			0.27
$(H-1)_d \rightarrow (L+4)_d$					−0.21	0.15	−0.17	−0.15	−0.20
$(H-5)_d \rightarrow (L+1)_d$								−0.26	
$H_d,H_d \rightarrow L_d,L_d$		0.17	0.25						0.31
$H_d,H_d \rightarrow L_d,(L+1)_d$			0.34				−0.16		0.19
$(H-1)_d,H_d \rightarrow L_d,L_d$								0.25	0.23
$F_d \rightarrow E_l/F_l \rightarrow E_d$									
$(H-2)_l \rightarrow L_d$						0.51	0.43		
$H_d \rightarrow (L+3)_l$						−0.29	−0.23		
$(H-1)_d \rightarrow (L+3)_l$									0.21
$(H-2)_l \rightarrow (L+1)_d$						0.32	0.25		
$F_l \rightarrow E_l$									
$(H-2)_l \rightarrow (L+3)_l$		0.17		−0.30		−0.24	0.27	0.22	
$(H-3)_l \rightarrow (L+2)_l$				0.21	0.17	−0.25	0.30	0.43	

The electronic configurations are denoted $F_d \rightarrow E_l$, where F [E] represents an occupied [unoccupied] Hartree–Fock molecular orbital (H stands for HOMO, L for LUMO) and the index d [l] is set for a delocalized [localized] orbital (see text).
We also include the transition dipole moments with the ground state, μ_{0i} (in D), the state dipole moment differences, $\mu_{ii} - \mu_{00}$ (in D), and the excitation energies, E_{0i} (in eV).

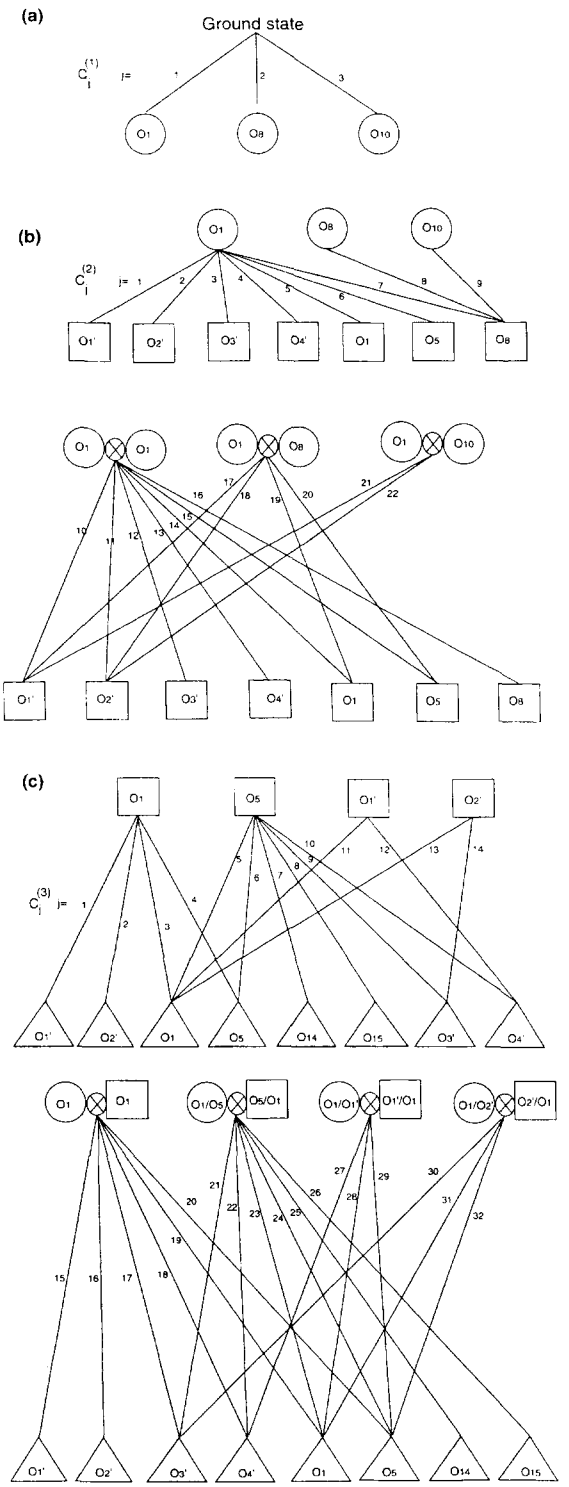

band (electron–electron and hole–hole) excitations and are, therefore, characterized by low frequencies ($\Omega = 0$ for O'_1 and O'_2). Although their physical meaning is still unclear, it seems likely that O'_1 and O'_2 should be related to the processes involving the state dipole moment differences in the SOS expressions. Indeed, as these processes do not require any electronic excitation, they have zero frequencies and can thus be regarded as a "propagation along the ground state or an excited state" (in contrast to an electronic transition between two states). In a similar way, O'_1 [O'_2] corresponds to a virtual HOMO → HOMO [LUMO → LUMO] process, that does not modify the original state of the system and does not give rise to any resonant peak in the frequency-dependent curves. The analogy is further supported by the fact that O'_1 and O'_2 contribute to the optical response mainly because of huge dipole moments (that, in this case, correspond to permanent dipoles). O'_3 and O'_4 are formed by the intraband HOMO → HOMO − 1 and LUMO → LUMO + 1 transitions. In contrast to interband-type oscillators, which in the SOS formalism correspond to excitations from the ground state to an excited state, O'_3 and O'_4 can be viewed as transitions among the excited states of the system. Indeed, with respect to the S_1 excited state described by the HOMO → LUMO excitation, the other essential states (coupled to S_1 through large transition dipole moments) are built by allowing the hole [electron] to hop from the HOMO [LUMO] level to the HOMO − 1 [LUMO + 1] level. Such hopping processes are precisely those dominating the description of O'_3 and O'_4. Note that, in the case of octatetraene, we found oscillators of the very same nature than O'_3 and O'_4, that play a major role in the expression of the off-resonance third-order response [24].

Fig. 7. Tree diagrams for the couplings, $C_j^{(n)}$, between the relevant oscillators in the description of the nth-order polarizability of DANS. Circles, squares, and triangles represent first-, second-, and third-order oscillators, respectively. The oscillators are classified in two categories (see text): (i) interband oscillators, formed by electron–hole excitations (labeled O_i); and (ii) intraband oscillators built from electron–electron or/and hole–hole pairs (labeled O'_i). Lines represent couplings and crosses denote the product of two oscillators. The contributions associated to these couplings are given in Table 4.

(iii) As in the SOS calculations, the contributions to the optical nonlinearities associated to other oscillators are about one order smaller and involve mainly O_5, O_8, O_{10}, O_{14}, and O_{15}. The HOMO − 1 → LUMO and HOMO → LUMO + 1 excitations dominating the description of O_5 are splitted in the INDO/MRD-CI calculations to give rise to the S_3 and S_5 excited states. At higher energy, transitions

Table 4
Contributions of the main couplings, $C_j^{(n)}$, to the static values of: (a) the nth-order oscillator amplitude; and (b) the nth-order polarizability of DANS, as calculated by the PPP/CEO scheme

$n=1$				$n=3$			
O_i	$C_j^{(1)}$	(a) (in 10^{-1})	(b) (in 10^{-1} e Å^2 V^{-1})	O_i	$C_j^{(3)}$	(a) (in 10^{-2})	(b) (in 10^{-2} e Å^4 V^{-3})
O_1	$j=1$	7.2	20.3	O'_1	$j=1$	6.8	12
O_8	$j=2$	1.3	1.1	O'_1	$j=15$	−0.94	−1.7
O_{10}	$j=3$	2.7	5.1	O'_2	$j=2$	6.8	21
$C_\Sigma^{(1)}$ (in 10^{-1} e Å^2 V^{-1})			26.5	O'_2	$j=16$	−0.93	−2.9
$C_{tot}^{(1)}$ (in 10^{-1} e Å^2 V^{-1})			27.0	O'_3	$j=9$	−21	−86
$n=2$				O'_3	$j=14$	34	139
O_i	$C_j^{(2)}$	(a) (in 10^{-2})	(b) (in 10^{-2} e Å^3 V^{-2})	O'_3	$j=17$	−1.3	−5.3
O'_1	$j=1$	−14	−25	O'_3	$j=21$	−3.0	−12
O'_1	$j=10$	1.4	2.5	O'_3	$j=30$	−2.9	−12
O'_1	$j=17$	0.43	0.78	O'_4	$j=10$	−21	−87
O'_1	$j=21$	0.31	0.56	O'_4	$j=12$	35	146
O'_2	$j=2$	−13	−41	O'_4	$j=18$	−1.3	−5.4
O'_2	$j=11$	1.4	4.4	O'_4	$j=22$	−3.0	−13
O'_2	$j=18$	0.38	1.2	O'_4	$j=27$	−2.7	−11
O'_2	$j=22$	0.34	1.1	O_1	$j=3$	5.0	14
O'_3	$j=3$	6.4	26	O_1	$j=5$	18	51
O'_3	$j=12$	−2.8	−11	O_1	$j=11$	−7.0	−20
O'_4	$j=4$	5.6	23	O_1	$j=13$	−6.9	−19
O'_4	$j=13$	−2.6	−11	O_1	$j=19$	−0.33	−0.93
O_1	$j=5$	−21	−59	O_1	$j=23$	0.85	2.4
O_1	$j=14$	0.7	2.0	O_1	$j=28$	0.43	1.2
O_1	$j=19$	0.4	1.1	O_1	$j=31$	0.421.2	
O_5	$j=6$	34	2.5	O_5	$j=4$	−8.0	−0.59
O_5	$j=15$	−6.1	−0.45	O_5	$j=6$	−9.3	−0.69
O_5	$j=20$	−0.73	−0.05	O_5	$j=20$	0.29	0.02
O_8	$j=7$	5.0	4.2	O_5	$j=24$	0.90	0.07
O_8	$j=8$	−1.7	−1.4	O_5	$j=29$	0.30	0.02
O_8	$j=9$	1.6	1.4	O_5	$j=32$	0.47	0.04
O_8	$j=16$	−0.98	−0.83	O_{14}	$j=7$	−9.1	−1.2
$C_\Sigma^{(2)}$ (in 10^{-2} e Å^3 V^{-2})			−79.0	O_{14}	$j=25$	1.3	0.17
$C_{tot}^{(2)}$ (in 10^{-2} e Å^3 V^{-2})			−65.0	O_{15}	$j=8$	−9.9	−2.4
				O_{15}	$j=26$	1.5	0.36
				$C_\Sigma^{(3)}$ (in 10^{-2} e Å^4 V^{-3})			107.0
				$C_{tot}^{(3)}$ (in 10^{-2} e Å^4 V^{-3})			93.0

We also indicate for each order in the field the sum, $C_\Sigma^{(n)}$, of the contributions associated to the dominant interband (O_i) and intraband (O'_i) oscillators and the total response, $C_{tot}^{(n)}$.
The couplings are labeled according to Fig. 7.

involving the two types of molecular levels (delocalized and localized orbitals) mix up and lead to the O_8, O_{10}, O_{14}, and O_{15} oscillators, that can be related to the high-energy band of excited states composed of S_6, S_8, S_9, S_{10}, S_{11}, and S_{15}. Although a one-to-one correspondence between the excited states and oscillators is rather tedious to establish in view of the complexity of their wavefunctions, we stress that the Hartree–Fock molecular orbital representation of O_{14} and O_{15}, with a large weight associated to the HOMO − 1 → LUMO + 1 transition and important contributions provided by the mixed-type (from delocalized to localized orbitals, and vice versa) excitations, compares well with that of S_9, S_{10}, S_{11}, S_{12}, and S_{15}. Oscillators O_8 and O_{10}, which include electronic transitions between orbitals confined on the benzene rings as well as excitations involving deep delocalized levels, present wavefunctions similar to S_6 and S_8.

To summarize, the comparison between the SOS and CEO results at the static limit shows that the essential excited states and oscillators dominating the linear, quadratic, and cubic response of DANS share a common origin. We now turn to the dynamic response. We have performed a similar analysis of the molecular polarizabilities for various values of the perturbing radiation field frequency, ω. This analysis has allowed us to assign the different resonant peaks calculated for the linear absorption spectrum and the second- and third-harmonic generation frequency-dependent curves, as shown in Table 6.

All the relevant excited states/oscillators in the

Table 5
Main coefficients in the expansion of the relevant interband (O_i) and intraband (O'_i) oscillators, dominating the optical response of DANS, as obtained from the PPP/CEO scheme

	O_1	O_5	O_8	O_{10}	O_{14}	O_{15}	O'_1/O'_2	O'_3/O'_4
Ω_i	3.95	5.97	6.45	7.24	7.78	7.79	0.0/0.0	1.65/1.67
$F_d \rightarrow E_d$								
$H_d \rightarrow L_d$	0.93	−0.26						0.29/−0.28
$(H-1)_d \rightarrow L_d$	0.18	0.63	0.15				−0.20	
$H_d \rightarrow (L+1)_d$	0.18	0.63					0.20	
$(H-1)_d \rightarrow (L+1)_d$	−0.16		0.35	−0.29	−0.52	0.59		
$(H-4)_d \rightarrow L_d$			0.27	−0.29	0.24	−0.28		
$H_d \rightarrow (L+4)_d$		−0.17	0.29	−0.52	0.24	−0.26		
$F_d \rightarrow E_1/F_1 \rightarrow E_d$								
$H_d \rightarrow (L+2)_1$			−0.26					
$H_d \rightarrow (L+3)_1$			0.17					
$(H-2)_1 \rightarrow L_d$			0.19					
$(H-3)_1 \rightarrow L_d$			−0.42					
$(H-1)_d \rightarrow (L+2)_1$					0.30	0.32		
$(H-2)_1 \rightarrow (L+1)_d$					0.58	0.47		
$(H-2)_1 \rightarrow (L+4)_d$					0.23	0.21		
$(H-4)_d \rightarrow (L+2)_1$					−0.16	−0.18		
$F_1 \rightarrow E_1$								
$(H-2)_1 \rightarrow (L+2)_1$			0.45	0.42				
$(H-3)_1 \rightarrow (L+3)_1$			0.35	0.57				
$F_d \rightarrow F_d/E_d \rightarrow E_d$								
$H_d \rightarrow H_d$							0.97	
$L_d \rightarrow L_d$							0.97	
$H_d \rightarrow (H-1)_d$								0.93
$L_d \rightarrow (L+1)_d$								0.93

The electronic excitations are denoted as in Table 3.
We also include the eigenenergies, Ω_i (in eV), of the oscillators.

description of the THG resonant peaks also lead to well-defined features in the optical absorption spectrum and the SHG dispersion curve. We will thus focus on the results obtained for the THG process. These results can be summarized as follows.

(i) The dominant S_1 excited state gives rise to intense three-, two-, and one-photon resonances (respectively, 3A, 3B″, and 3E on Fig. 5a). Similarly, peaks 3a, 3b, and 3e on Fig. 5b are associated to resonances to the corresponding oscillator, O_1.

(ii) Peak 3b has also important contributions from oscillator O_5. As pointed out before, O_5 is splitted in the INDO/MRD-CI description and leads to the S_3 and S_5 excited states, responsible for peaks 3B and 3B' in the SOS simulated THG curve (Fig. 5a).

(iii) In the THG spectrum obtained within the CEO scheme, peak 3c (Fig. 5b) results from the superimposition of three-photon resonance to O_{14} and O_{15}, and to a smaller extent O_8 and O_{10}. In this energy domain of the dispersion curve, excited states S_9, S_{10}, S_{11} and S_{15} dominate the cubic nonlinearity and lead to resonant peaks 3C and 3C′ (Fig. 5a); S_6 and S_8 also participate to feature 3C.

(iv) The important excited states giving rise to the mean features (3C and 3C′) on the SOS third-harmonic generation frequency-dependent curve between 2.0 and 2.5 eV are also involved in two-photon resonances, contributing to peak 3E. In a similar way, oscillators O_{14} and O_{15}, responsible for peak 3C on the CEO spectrum, also show up in the expression of the THG response around 4.0 eV (peak 3e).

These results fully support the connection established between the dominant excited states and oscil-

Table 6
Assignment of the main resonant peaks in the linear optical absorption (OA), second-harmonic generation (SHG), and third-harmonic generation (THG) spectra of DANS, as simulated at the INDO/MRD-CI/SOS and PPP/CEO levels

SOS		CEO	
peak	assignment	peak	assignment
OA			
1A	S_1 (1)	1a	O_1 (1)
1B	S_3 (1)	1b	O_5 (1)
1B′	S_5 (1)		
1C	S_6 (1), S_8 (1), S_9 (1), S_{10} (1)	1c	O_8 (1)
1D	S_{11} (1)	1d	O_{10} (1)
1E	S_{15} (1)	1e	O_{14} (1), O_{15} (1)
SHG			
2A	S_1 (2)	2a	O_1 (2)
2B	S_3 (2)	2b	O_5 (2)
2B′	S_5 (2)		
2C	S_6 (2), S_8 (2)	2c	O_8 (2)
2D	S_9 (2), S_{10} (2), S_{11} (2), S_{15} (2)	2d	O_{10} (2), O_{14} (2), O_{15} (2), O_1 (1)
2D′	S_1 (1)		
THG			
3A	S_1 (3)	3a	O_1 (3)
3B	S_3 (3)	3b	O_5 (3), O_1 (2)
3B′	S_5 (3)		
3B″	S_1 (2)		
3C	S_8 (3), S_9 (3), S_{10} (3)	3c	O_8 (3), O_{10} (3), O_{14} (3),O_{15} (3)
3C′	S_{11} (3)		
3D	S_{15} (3), S_3 (2)	3d	O_5 (2)
3E	S_{10} (2), S_{11} (2), S_{15} (2), S_1 (1)	3e	O_{14} (2), O_{15} (2), O_1 (1)

The peaks are labeled according to Figs. 3–5.
The relevant excited states/oscillators are indicated for the different frequency domains considered; the numbers between parentheses specify the nature of the resonance (1 = one-photon resonance; 2 = two-photon resonance; 3 = three-photon resonance).

lators uncovered by the analysis of the static response.

5. Conclusions

The linear and nonlinear optical polarizabilities of DANS have been evaluated on the basis of a coupled electronic oscillator (CEO) picture and compared to the results of sum-over-states (SOS) calculations. We found a very good agreement between the static values of the first-, second-, and third-order polarizabilities obtained by the two techniques; the overall shapes of the linear absorption and second- and third-harmonic generation dispersion curves simulated within the CEO formalism also compare well to those of the corresponding spectra calculated by the SOS scheme.

We have unraveled the nature of the relevant oscillators/excited states in the description of the nonlinearities. In the CEO picture, oscillators couple with the external electric field and among themselves to lead to various contributions to the quadratic and cubic responses. In the SOS representation, the polarizabilities are expressed in terms of channels involving transition dipole moments and state dipole moment differences between the eigenstates. Although they present common features, there is no obvious one-to-one correspondence between the important pathways in the CEO description and the relevant channels in the SOS formalism (note that this correspondence appears more clearly in the case of octatetraene where the number of dominant pathways/channels is very much reduced [24]). However, by projecting the eigenstates/oscillators onto the Hartree–Fock molecular orbitals, we found a clear connection between the dominant oscillators and the essential excited states. The assignment of the resonant peaks in the SHG and THG dispersion curves further supports the analogy.

Comparison between SOS and CEO results is extremely useful not only to provide a unified description of the nonlinear optical response in conjugated systems but also to estimate the accuracy of the coupled electronic oscillator picture versus the well-established sum-over-states formalism. This is important since the CEO method has two major advantages over the SOS approach: (i) it is, by far, less computationally demanding; and (ii) it is size consistent and can thus be applied to much longer conjugated chains.

Acknowledgements

The work in Mons has been partly supported by the Belgian Government Services Fédéraux des Affaires Scientifiques, Techniques et Culturelles (Pôle d'Attraction Interuniversitaire No. 16: Chimie Supramoléculaire et Catalyse), FNRS/FRFC, and an IBM Academic Joint Study; this work is conducted in the framework of the Commission of European Union ESPRIT Network of Excellence on Organic Materials for Electronics (NEOME) and Human Capital Mobility Networks Synthetic Organic Materials (SELMAT) and New Third-Order Nonlinear Optical Molecular Materials. The work in Rochester has been supported by the Air Force Office of Scientific Research and the National Science Fundation. DB is Chargé de Recherches of the Belgian National Fund for Scientific Research (FNRS).

References

[1] D.S. Chemla and J. Zyss, eds., Nonlinear optical properties of organic molecules and crystals (Academic, New York, 1987).

[2] J.L. Brédas and R.R. Chance, eds., Conjugated polymeric materials: opportunities in electronics, optoelectronics, and molecular electronics, NATO-ARW Series E182 (1990); J. Messier, F. Kajzar and P. Prasad, eds., Organic molecules for nonlinear optics and photonics, NATO-ASI Series E194 (1991); D.J. Williams and P. Prasad, eds., Introduction to nonlinear optical effects in molecules and polymers (Wiley-Interscience, New York, 1991).

[3] S.R. Marder, J.E. Sohn and G.D. Stucky, eds., Materials for nonlinear optics: chemical perspectives, ACS Symp. Series (1991).

[4] J.L. Brédas, C. Adant, P. Tackx, A. Persoons and B.M. Pierce, Chem. Rev. 94 (1994) 243.

[5] B.J. Orr and J.F. Ward, Mol. Phys. 20 (1971) 513.

[6] J.M. André, J. Delhalle and J.L. Brédas, eds., Quantum chemistry aided design of organic polymers. An introduction to the quantum chemistry of polymers and its applications (World Scientific, Singapore, 1991).

[7] H.A. Kurtz, J.J.P. Stewart and K.M. Dieter, J. Comput. Chem. 11 (1990) 82.

[8] F. Sim, S. Chin, M. Dupuis and J. Rice, J. Phys. Chem. 97 (1993) 1158.

[9] P.S. Karna, Z. Laskowski, G.B. Talapatra and P.N. Prasad, J. Phys. Chem. 95 (1991) 6508.
[10] A.F. Garito, J.R. Heflin, K.Y. Wong and O. Zamani-Khamiri, in: Organic materials for nonlinear optics, eds. R.A. Hann and D. Bloor (Roy. Soc. Chem., London, 1989) p. 16.
[11] P.C.M. McWilliams, G.W. Hayden and Z.G. Soos, Phys. Rev. B 43 (1991) 9777.
[12] D. Guo, S. Mazumdar, S.N. Dixit, F. Kajzar, Y. Kawabe and N. Peyghambrian, Phys. Rev. B 48 (1993) 1433.
[13] D. Beljonne, Z. Shuai and J.L. Brédas, J. Chem. Phys. 98 (1993) 8819; Z. Shuai, D. Beljonne and J.L. Brédas, J. Chem. Phys. 97 (1992) 1132.
[14] Z.G. Soos and D. Mukhopadhyay, J. Chem. Phys. 101 (1994) 5515.
[15] D. Beljonne and J.L. Brédas, J. Opt. Soc. Am. B 11 (1994) 1380.
[16] D. Beljonne, J.L. Brédas, M. Cha, W.E. Torruellas, G.I. Stegeman, J.W. Hofstraat, W.H.G. Horsthuis and G.R. Möhlmann, J. Chem. Phys. 103 (1995) 7834.
[17] D. Guo, S. Mazumdar, G.I. Stegeman, M. Cha, D. Neher, S. Aramaki, W.E. Torruellas and R. Zanoni, Mater. Res. Soc. Symp. Proc. 247 (1992) 151.
[18] B.M. Pierce, J. Chem. Phys. 91 (1989) 791.
[19] A. Takahashi and S. Mukamel, J. Chem. Phys. 100 (1994) 2366.
[20] S. Mukamel and H.X. Wang, Phys. Rev. Letters 69 (1992) 65; S. Mukamel, A. Takahashi, H.X. Wang and G. Chen, Science 266 (1994) 251.
[21] G. Chen and S. Mukamel, J. Am. Chem. Soc. 117 (1995) 4945; J. Chem. Phys. 103 (1995) 9355.
[22] D.J. Rowe, Rev. Mod. Phys. 40 (1968) 153.
[23] H. Sekino and R.J. Bartlett, J. Chem. Phys. 85 (1986) 976.
[24] G. Chen, S. Mukamel, D. Beljonne and J.L. Brédas, J. Chem. Phys., in press.
[25] W.E. Torruellas, R. Zanoni, G.I. Stegeman, G.R. Möhlmann, E.W.P. Erdhuisen and W.H.G. Horsthuis, J. Chem. Phys. 94 (1991) 6851; M. Cha, W.E. Torruellas, G.I. Stegeman, W.H. Horsthuis, G.R. Möhlmann and J. Meth, Appl. Phys. Letters 65 (1994) 2648.
[26] M.J.S. Dewar, E.G. Zoebisch, E.F. Healy and J.J.P. Stewart, J. Am. Chem. Soc. 107 (1985) 3902.
[27] J. Ridley and M. Zerner, Theoret. Chim. Acta 32 (1973) 111.
[28] R.J. Buenker and S.D. Peyerimhoff, Theoret. Chim. Acta 35 (1974) 33.
[29] P. Tavan and K. Schulten, J. Chem. Phys. 85 (1986) 6602.
[30] A. Wiletts, J.E. Rice, D.M. Burland and D.P. Shelton, J. Chem. Phys. 97 (1992) 7590.
[31] S.R. Marder, D.N. Beratan and L.T. Cheng, Science 252 (1991) 103.
[32] J. Cornil, D. Beljonne, R.H. Friend and J.L. Brédas, Chem. Phys. Letters 223 (1994) 82.
[33] D. Beljonne, F. Meyers and J.L. Brédas, submitted for publication.
[34] J.L. Oudar, Phys. Rev. A 26 (1982) 2016; J.L Oudar and D.S. Chemla, J. Chem. Phys. 66 (1977) 2664.
[35] G. Chen and S. Mukamel, Chem. Phys. Letters 240 (1995) 296.